Heliyon 10 (2024) e31854

Contents lists available at ScienceDirect

Heliyon

journal homepage: www.cell.com/heliyon

Research article

Titania-zeolite composite for tetracycline photocatalytic degradation under visible light: A comparison between doping and ion exchange

Ghadeer Jalloul [a,*], Nour Hijazi [b], Cassia Boyadjian [a], Hussein Awala [b], Ahmad B. Albadarin [a], Mohammad N. Ahmad [a]

[a] Baha and Walid Bassatne Department of Chemical Engineering and Advanced Energy, Maroun Semaan Faculty of Engineering and Architecture, American University of Beirut, Beirut, Lebanon

[b] Lebanese University, Laboratory of Inorganic and Organometallic Coordination Chemistry (LCIO), Faculty of Science, Hadath, Lebanon

ARTICLE INFO

Keywords:
Antibiotic
Visible light photocatalysis
Immobilized TiO_2
Iron-doped TiO_2
Ion-exchanged zeolite

ABSTRACT

In this study, TiO_2 supported over embryonic Beta zeolite (BEA) was prepared for the photocatalytic degradation of Tetracycline (TC) antibiotic under visible light. The immobilization of sol-gel TiO_2 over the zeolite increased its surface area from 33 (m^2/g) to 226 (m^2/g) and enhanced its adsorption efficiency from 8 % to 18 %. In order to expand the photocatalytic activity of TiO_2 towards the visible light region (i.e. $\lambda > 380$ nm), two different metal sensitization techniques with Iron ions from aqueous solution of $FeCl_3$ were explored. In the ion-exchange method, the substitutional cations within the TiO_2/BEA structure were exchanged with Fe^{3+}. Whereas, in the doping technique, solgel TiO_2 was doped with Fe^{3+} during its synthesis and before its immobilization over Zeolite. Four different samples with 20, 40, 60, and 100 % w/w of TiO_2/BEA ratio were prepared. After testing the various ion-exchanged photocatalysts under blue and white lights, only Fe–60%TiO_2/BEA showed better activity compared to pure TiO_2 under white light at TC initial concentration, $C_o = 20$ ppm. For the doped immobilized Titania with 60 wt% TiO_2/BEA, three different doped photocatalysts were prepared with 3 %, 7 %, and 10 % per mole Fe/TiO_2. All the Fe-doped TiO_2/BEA photocatalysts showed better activity compared to pure TiO_2 under white light. Under solar irradiations, the 3 % Fe-doped TiO_2/BEA was able to degrade all TC within 120 min, while Fe–60%TiO_2/BEA needed 200 min, and TiO_2 needed more than 300 min. This enhanced performance was a result of both increased surface area due to immobilization over BEA as well as iron doping by Fe^{3+} that simultaneously increased the visible light absorption of TiO_2 and minimized the charge carrier recombination effect.

1. Introduction

Antibiotic resistance is a concerning health threat affecting various species on the planet, including humans. The main reason behind this issue is the continuous discharge of antibiotics into the environment through untreated wastewater from hospitals, sewage, poultry, and livestock [1–3]. Tetracyclines are a group of antibiotics including chlortetracycline, oxytetracycline, tetracycline

* Corresponding author.
E-mail address: gaj08@mail.aub.edu (G. Jalloul).

https://doi.org/10.1016/j.heliyon.2024.e31854
Received 6 February 2024; Received in revised form 17 May 2024; Accepted 22 May 2024
Available online 27 May 2024

hydrochloride, and tetracycline. Tetracyclines are the second most used antibiotic group worldwide wide due to their wide antimicrobial spectrum and low cost [2,4]. Heterogeneous photocatalysis used under solar light has gained interest in the last few years for degrading organic pollutants including pharmaceuticals as an ecofriendly technology [5]. For the photocatalyst, TiO_2 was reported as the best semiconductor to be employed for such application due to its low cost, non-toxicity, and stability [1,5]. However, TiO_2 is highly active only under UV light due to its large band gap energy, and therefore it requires modifications to increase its visible light absorption and photocatalytic efficiency [6]. Metal doping has been proven to lower the band gap energy of TiO_2 and increase its activity under solar light [6–8]. Ferric ion is known for its half occupied electronic d-shell ($3\ d^5$) with an ionic radius of 0.064 nm which is almost the same as that of TiO_2 (0.068 nm) allowing it to be doped into the lattice structure of TiO_2 [6]. For example, Tsiampalis et al. applied Fe-doped TiO_2 for the photocatalytic degradation of sulfamethoxazole antibiotic under simulated solar radiation and reported the highest efficiency (95 % after 120 min) by the sample having 0.04 % molar ratio of Fe ions. The main reason for the enhanced activity of Titania was its lower band gap energy compared to TiO_2 as a result of the formation of the dopant energy level of Fe^{2+}/Fe^{4+} and the d-d transition of the ferric ions. Similarly, Ghoreishian et al. [9] prepared Fe–Sn co-doped TiO_2 nanofibers for the degradation of tetracycline under 300 W xenon (Xe) lamp and reported a 96.96 % removal of TC, which was 1.86 times higher than the degradation efficiency of pristine TiO_2. This improvement in the performance due to the doping was attributed to the lower band gap energy and suppressed charge carrier recombination effect. To increase the surface area and adsorption efficiency of TiO_2, it is widely immobilized over inert porous non-organic substrates to help enhance the interactions between its active sites and the target molecules [10–13]. Zeolite is a porous material consisting mainly of aluminum and silica with a tetrahedron three-dimensional morphology, high surface area and pore volume, inertness, excellent stability, and transparency to light [7,14–18]. However, zeolites suffer from limited mass transfer due to low accessibility of their micropores. Researchers are now developing mesoporous amorphous zeolite prepared in a shorter time, with partially formed structures and larger pore opening to shorten the diffusion route into active sites, known as embryonic zeolites [19–21]. Embryonic zeolites are widely used as catalysts for various applications including 1,3,5-triisopropylbenzene dealkylation, synthesis of dimethyl ether, and removal of NOx [18,19,21]. Amorphous zeolites are easier and faster to prepare compared to fully crystalline zeolites. Various studies have reported preparing TiO_2/zeolite photocatalysts for organic material degradation under visible light. For example, Foura et al. [7] used an Fe-doped TiO_2/zeolite photocatalyst for methylene blue dye degradation under visible light and reported a degradation activity of (98 %) as compared to TiO_2/zeolite (30 %) after 60 min. The study reported remarkable enhancement of 60 % in the adsorption efficiency of the final immobilized Titania as compared to TiO_2. The enhanced photocatalytic degradation of the Iron-doped TiO_2/zeolite was attributed to the increase in the surface area of this composite in addition to the improved visible light absorbance, as the iron content increased from 3 % to 10 %. Similarly, Rahman et al. [17] employed TiO_2/mordenite natural zeolite for the photocatalytic degradation of methyl orange dye under solar light irradiations. In this work, the Titania-zeolite composites with various TiO_2 contents had higher band gap energies compared to pure TiO_2 as a result of quantum size effect. However, complete removal of the dye was accomplished after 200 min by 10 % TiO_2/zeolite compared to only 85 % by TiO_2. In another study by Saadati et al. [22], TiO_2/semnan natural zeolite was tested for the photocatalytic degradation of tetracycline antibiotic, and an enhancement in the surface area of TiO_2 by 2 times and 87 % degradation after 90 min were reported. In this study, the immobilization of Titania over the zeolite lowered its band gap energy from 3.2 to 2.4 eV and improved its adsorption capacity. On the other hand, Kanakaraju et al. [23] also applied TiO_2/zeolite for the photocatalytic degradation of Amoxicillin antibiotic and the complete removal was attained after 240 min. Liu et al. [24] studied the ability of TiO_2/Fe_2O_3/zeolite to degrade ciprofloxacin antibiotic under visible LED light in the presence of persulfate. At pH 7 and 1 g/L of the catalyst dosage the Titania composite was able to completely degrade the antibiotic after 120 min in the presence of 5 mM of persulfate. This excellent efficiency of the photocatalyst was attributed to minimized charge carrier recombination effect and enhanced visible light activity. In our previous work [10], we prepared highly crystalline embryonic Beta zeolite (BEA) to be used as a support for TiO_2 for the photocatalysis of antibiotics. However, the preparation of this meso-porous zeolite via a seed-assisted approach required a 3-day duration for the seed preparation followed by a 5-day thermal treatment for the BEA zeolite preparation. In the current study, we report the preparation of embryonic amorphous BEA zeolite using tetraethylammonium hydroxide precursor under 3 days and its utilization, for the first time, as a catalyst support. Particularly, we immobilized solgel TiO_2 over embryonic BEA zeolite and studied its ability to be employed as an efficient Titania support in the photocatalytic degradation of tetracycline (TC) antibiotic. The weight of TiO_2 was varied from 20 % to 100 % to optimize the TiO_2 percentage i.e., zeolite ratio in the final photocatalyst. Two methods to sensitize this photocatalyst by ferric ions were used to enhance its visible light absorption. The performance of the ion-exchanged and the doped Titania/zeolite composites were compared under blue, white, and real solar radiations.

2. Materials and methods

2.1. Materials and chemicals

Titanium (IV) n-butoxide (>98 %, Acros Organics), colloidal silica: Ludox HS, (Sigma-Aldrich, 30 % SiO_2, particle size 3–4 nm), sodium aluminate (Sigma-Aldrich), tetraethylammonium hydroxide (Sigma-Aldrich, 35 %), ethanol (Fisher Chemical, 99 %), nitric acid (BDH Laboratory supplies, 69 %), sodium hydroxide (Sigma-Aldrich), Tetracycline (Sigma-Aldrich), Iron (III) anhydrous chloride (BDH Laboratory supplies). All chemicals were used without further purification.

2.2. Preparation of the photocatalysts

2.2.1. Preparation of TiO_2 sol-gel

TiO_2 was prepared using the sol-gel method as described previously [10]. Two mixtures **A** and **B** were separately prepared before being mixed. Mixture **A** contained 4 mL of titanium (IV) butoxide and 2 mL of ethanol that were stirred for 30 min. Mixture **B** was composed of 0.4 mL of nitric acid, 2 mL H_2O, and 17 mL of ethanol. Mixture **B** was gradually added into mixture **A** using a dropper (approximately 3 mL/min) under vigorous stirring until the clear solution turned into a white gel. The obtained gel was then dried in an oven at 80 °C for 3 h to remove any remaining water or ethanol. The obtained solid was first grinded then calcined in a muffle furnace for 5 h at 450 °C to induce the crystallization of TiO_2.

2.2.2. Preparation of BEA zeolite

BEA zeolite was prepared from clear precursor suspensions of tetraethylammonium hydroxide with molar compositions: 9TEAOH: $0.5Al_2O_3$: $25SiO_2$: $295H_2O$ in distilled water. First, the sodium aluminate was dissolved in TEAOH solution then the colloidal silica source (Ludox SM 30 % by weight) was added to the mixture while being stirred. After mixing the chemicals for 60 min, a hydrothermal treatment was carried out at 100 °C for 3 days. High speed multistep centrifugation (10,000 rpm, 90 min) was used to purify the resulting suspensions. The collected solid product was then dried at 50 °C for 3 h and calcined at 550 °C for 6 h to be used as a photocatalyst support.

2.2.3. Modification of the TiO_2 sol-gel

2.2.3.1. Preparation of TiO_2/BEA. The preparation of TiO_2/BEA photocatalyst was performed during the synthesis of the TiO_2 sol-gel. An appropriate amount of zeolite was added into the clear TiO_2 sol-gel suspension after adding mixture B into mixture A. After the formation of the white gel, it was dried in oven at 80 °C for about 4 h then moved into a furnace at 450 °C for 4 h. TiO_2/BEA catalysts were prepared with 20 %, 40 %, 60 %, and 100 % w/w of TiO_2. Here, 60TZ refers to a photocatalyst having 60 % w/w ratio of TiO_2/BEA. This sample was prepared to study the effect of Fe ions presence in enhancing the visible light absorption in the final catalysts, having the same weight percentage of TiO_2.

2.2.3.2. Preparation of ion-exchanged Fe–TiO_2/BEA. The zeolite supported TiO_2 (TiO_2/BEA) was further subjected to an ion exchange treatment to incorporate Fe ions into the final catalyst. For this, 1.0 g of TiO_2/BEA powder was added to 40 mL of 0.05 M iron chloride ($FeCl_3$) solution and stirred for 20 min. The ion exchange step was repeated three times to ensure the highest possible exchange of the Fe ions. Specifically, the solid product was separated each time from the solution and then added into a fresh new solution of $FeCl_3$. The recovered solid product from ion exchange was washed twice with double deionized water then dried in the oven at 80 °C for 4 h. The final dried sample was then calcined in a muffle furnace at 450 °C for 4 h. The final obtained ion exchanged sample was named XFeTZ where Z is the weight percentage of TiO_2 with respect to the zeolite and X can be 20 %, 40 %, 60 %, or 100 %.

2.2.3.3. Preparation of Fe-doped TiO_2/BEA. For Fe-doped TiO_2/BEA, a doping solution composed of an appropriate amount of anhydrous iron chloride dissolved in 8 mL of distilled water was gradually added into solution A and heated at 70 °C followed by the gradual addition of mixture B. After that, an appropriate amount of the zeolite nanoparticles was added into the transparent sol-gel and the suspension was kept under stirring conditions until a white gel was formed. The final product was dried at 80 °C for about 4 h followed by calcination at 450 °C for 4 h. Three doped samples were prepared with different mole percentages of Fe/TiO_2. The samples were named as follows: 3FeTZ, 7FeTZ, and 10FeTZ where 3FeTZ corresponds to the sample with 3 % mol Fe/TiO_2 immobilized over the zeolite with the weight percentage of TiO_2/BEA being 60 %. The 60 % weight of TiO_2 in the doped samples was selected based on the photocatalytic degradation results of the ion-exchanged samples indicating that the 60 % weight resulted in the highest efficiency.

2.3. Catalyst characterization

X-ray powder diffraction (XRD) (BRUKER, D8) in the range of $5° < 2\theta < 80°$ with a step size of 0.02° was used to identify the crystalline phases of the various modified and non-modified samples. To determine the surface area and the pore volume of various prepared samples, Brunauer–Emmett–Teller (BET) was applied using (GEMINI VII 2390). In which, N_2 adsorption/desorption isotherms with the relative pressure range (P/P_0: 0.04–0.99) at 77 K were obtained. To investigate the morphology of the surface structure of the photocatalysts, scanning electron microscope (SEM) using MIRA3 LMU by TESCAN was applied with 5 kV analysis voltage. Prior to analysis, the samples were coated with Gold (20 nm) using sputtering machine by (Quoum, Q150T ES). Thermogravimetric analysis performed using TGA 209 Libra (Netzsch) using nitrogen was also applied to test the thermal stability of the different photocatalysts. Bruker Tenor 27 FT-IR was used to collect the Fourier transform infrared (FTIR) spectra (4000-400 cm^{-1}) of the catalysts and confirm the existing bonds.

2.4. Photocatalytic degradation experiments

For the photocatalytic degradation tests, the reactor setup was assembled using a 1 L plastic beaker fully covered with aluminum foil to prevent any light interaction from the surroundings. The beaker was initially filled with 300 mL of TC solution (Initial

concentration, $C_o = 20$ ppm) prepared the day before. 30 mg (equivalent to 100 mg/L catalyst loading) of the desired photocatalyst was added into the beaker and kept under moderate stirring using an 8 cm long magnetic bar to ensure perfect interaction between the photocatalyst's particles and TC molecules. After the addition of the catalysts, the system was kept under dark conditions for 30 min to ensure adsorption/desorption equilibrium of the tetracycline molecules on the surface of the photocatalyst, then the light was turned on. Two LED lights were used as a source of illumination to activate the electrons in the catalyst, a blue LED light ($450<\lambda<495$ nm) and a white LED light as a solar simulator. Solar reactions were performed in August in Beirut, Lebanon, American University of Beirut (**Latitude** 33.89 N, **Longitude:** 35.47603 E with average daily direct normal irradiation of 5.8 kWh/m^2) between 12 noon and 5 p.m. At specific times, a 2 mL sample was withdrawn from the system and added to a 15 mL Falcon tube, which was then centrifuged at 10,000 rpm for 10 min to separate the catalysts from the solution. The pure liquid was then added into new vials and analyzed by high performance liquid chromatography (HPLC) (AGILENT TECHNOLOGIES with ChemStation software). A C18 column (Viva 5 μ m, 150 $\times$ 4.6 mm) by RESTEK was used and the analysis was done at $\lambda = 357$ nm. Initially, a calibration curve was plotted to find the exact concentration of TC in each sample. For the calculation of the overall photocatalytic efficiency of the photocatalyst **Equation (1)** was applied. The adsorption tests were conducted in the system following the same procedures but in the absence of any light illumination.

$$TC\ degradation\ \% = \frac{C_0 - C_t}{C_0} \times 100 \quad (1)$$

Where C_o and C_t are the initial and final concentration of TC at time *t*, respectively.

3. Results and discussions

3.1. Characterization of the catalysts

3.1.1. Ion exchange method

3.1.1.1. XRD analysis and TGA. Fig. 1 shows the XRD patterns of BEA zeolite, TiO_2, and ion exchanged TiO_2/BEA photocatalysts. The XRD plot of the prepared zeolite showed two main broad peaks at $2\theta = 7.6°$ and 22.4° confirming the structure of the amorphous embryonic BEA zeolite [18]. The XRD diffraction patterns of TiO_2 showed peaks at $2\theta = 25.2°$, 36.98°, 48.4°, 54.9°, 62.7°, 68.8°, and 70.1° corresponding to the (101), (103), (200), (211), (204), (113), and (220) anatase phase planes, and 27.33°, 36°, and 41.2°, 44.1°, and 56.46° corresponding to (110), (101), (111), (210), and (220) for the rutile phase crystallographic planes based on (JCPDS 21–1272) and (JCPDS 21–1276) spectrum standards [25]. Accordingly, the sol-gel TiO_2 was observed in both anatase and rutile polymorphs consistent with those for solgel TiO_2 calcined under mild temperatures 200 °C < T < 550 °C [17,23,26–29]. The XRD diffraction patterns of the FeTZ catalysts and the unmodified 60TZ photocatalyst possessed very low crystallinity as compared to TiO_2. The main characteristic diffraction peaks for the TiO_2/BEA photocatalysts corresponded to the BEA zeolite at $2\theta = 7.6°$ and to anatase TiO_2 at $2\theta = 25°$, 36.98°, 48.4°, 54.9°, 62.7°. Therefore, both zeolite and TiO_2 were present in the final photocatalyst, drawing the same conclusion reported by other zeolite supported TiO_2 studies [7,15,22,24,27,29–32]. The typical peak of BEA at $2\theta = 7.6°$ remained in the TiO_2/BEA photocatalyst and its intensity increased confirming that the framework structure of the zeolite was conserved after the incorporation of Titania. This was a result of the incorporation of the TiO_2 particles on the surface of this zeolite rather than completely in the pores of the zeolite [7,15,16,22,24,27,29–32]. Based on Fig. 1, no additional peaks corresponding to iron ions were observed, and this provides clear proof that Fe ions performed an ion exchange with the sodium ions in the zeolite and did not form ferric oxide on the surface [5].

The TGA thermograms of the zeolite and the titania photocatalysts is shown in the supplementary data (Fig. S1). TiO_2 was the most stable photocatalyst between 35 °C and 1000 °C, while zeolite only lost 5 % of its initial weight when heated up to 200 °C without any additional loss at higher temperatures. Based on the TGA thermograms of the immobilized TiO_2 photocatalysts, the prepared photocatalysts were thermally stable between 35 °C and 1000 °C with weight loss of less than 5 %.

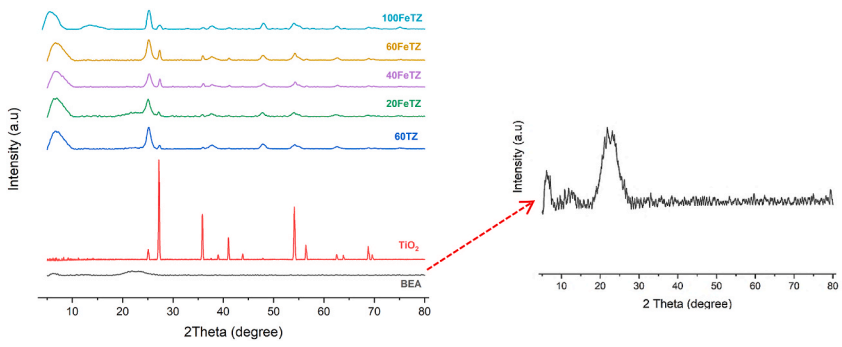

Fig. 1. XRD patterns of BEA zeolite, TiO_2, and TiO_2/BEA ion-exchanged photocatalysts.

3.1.1.2. Specific surface area (BET) and N_2 adsorption–desorption characterization. Table 1 presents the BET results of BEA zeolite, TiO_2, and Titania ion-exchanged photocatalysts. The BEA zeolite possessed the highest surface area and pore volume among the catalysts. After immobilizing TiO_2 on BEA, the surface area decreased (389.7–226.6 m^2/g) and pore volume of 60TZ also decreased (0.917–0.509 cm^3/g). This remarkable decrease in the pore volume and surface area was a result of mesopore clogging of the zeolite, only occurring when the pore diameter of zeolite is greater or equal to the titania particle size [26]. Maksod et al. [31], Liu et al. [29], and Foura et al. [7] reported a possible deposition of TiO_2 particles in the pore structure of the zeolite leading to a partial blocking. As the weight percentage of TiO_2 increased in the photocatalyst the surface area, as well as the pore volume, decreased. This was due to more deposition of TiO_2 particles into the pores of the zeolite. The 60FeTZ sample exhibited a surface area slightly lower than the surface area of 60TZ, 214 and 226.63 m^2/g, respectively; however, the latter had a higher pore volume (0.509 and 0.419 cm^3/g). This was due to ion exchange of the sodium ions in zeolites by iron ions that may have slightly altered the pore structure of zeolite as described in previous studies [33,34]. All the Titania ion exchanged photocatalysts possessed higher surface areas and pore volumes as compared to TiO_2, and this was consistent with what was reported in other studies [14,15,32,35]. This improvement of Titania's surface area would lead to enhanced tetracycline adsorption as discussed by Saadati et al. [26]. Fig. 2, shows the N_2 adsorption-desorption isotherms of the prepared photocatalysts. All the photocatalysts showed type IV isothermals with hysteresis loops according to IUPAC isotherm classifications due to capillary condensations experienced in the meso-pores [36]. Similarly, the same H2 hysteresis loop type was recorded for the BEA zeolite and the prepared photocatalysts as a result of zeolite particles agglomerates that led to the formation of those meso-pores. This suggest that the meso-pores structure of BEA zeolite was conserved after Titania immobilization and iron ion exchange [10].

3.1.1.3. FTIR. FTIR was performed for all the samples to analyze the interaction between Titania and the zeolite. The FTIR of the zeolite shown in Fig. S2 represents a typical spectrum of amorphous zeolite, confirming the bonds corresponding to Si, Al, and O elements. The spectrum of the zeolite showed a band in the 950–1250 cm^{-1} range corresponding to the antisymmetric stretching vibration of the Si–O bonds [7,29,37]; while the band between 440 and 470 cm^{-1} was for the Si–O bending vibrations in the zeolite. The peak at 790 cm^{-1} corresponded to the stretching of the vibrations Al–O [38]. The OH stretching and bending vibrations of silanol groups (Si–OH) were observed by the band at 3400 cm^{-1} while the 1600 cm^{-1} band was attributed to the bend vibrations of H–*O*–H bonds for the water molecules on the surface of the zeolite [33,39]. For TiO_2, a remarkable band was observed at 500 cm^{-1} corresponding to anatase titania and in agreement with the XRD of solgel TiO_2 [40]. Rahman et al. [17] reported the same FTIR spectrum for TiO_2 including two close bands for 2500 cm^{-1}. The spectrums of the ion-exchanged Titania photocatalysts possessed the same spectrum of the zeolite with lower intensities. As shown in Fig. S2, as the weight percentage of TiO_2 increased the intensity of the main peaks of BEA decreased because the amount of BEA in the photocatalyst decreased and this was reported elsewhere [17]. The intensity of the 60FeTZ spectrum was lower than those for the 60TZ photocatalyst, although they had the same weight percentage of TiO_2, this observation was reported by Bhat et al. [41] and was a result of metal ion exchange. The FTIR of the Titania photocatalysts showed a change in the shape of the spectrum between 500 cm^{-1} and 900 cm^{-1} caused by the strong interaction between TiO_2 and the porous surface of the zeolite through Ti–O–Si bonds [17,42]. The existence of this bond was characterized by a band located around 960 cm^{-1} and whose intensity is highly affected by the amount of Ti in the photocatalyst [28,39]. In our photocatalyst, a wide peak with low intensity was detected at 965 cm^{-1} as shown in Fig. S2. Based on other studies, the interaction between Titania crystalline particles and the surface of the porous zeolite may either be through chemical bonding or physical deposition [39]. Chong et al. [39] and Behravesh et al. [14] prepared TiO_2 immobilized over zeolite and observed no chemical bonding based on FTIR patterns, whereas Saadati et al. [22] and Rahman et al. [17] reported chemical bonding as Ti–O–Si and/or Ti–O–Al. In our work, this was an additional proof of the successful immobilization of Titania on the surface of zeolite through chemical bonds.

3.1.1.4. SEM surface morphology characterization. Fig. 3 shows the SEM images of all the prepared samples. The SEM images of the BEA zeolite, Fig. 3, a, showed indefinite morphology with a rough surface that was also observed in a study by Palcic et al. [18] and as expected based on the XRD pattern of the zeolite. Fig. 3, b, shows the structure of TiO_2 having a smooth surface and composed of aggregates with sharp edges in a similar finding by other studies [10,28]. The SEM images of the ion exchanged and the unmodified TiO_2/BEA in Fig. 3, c, d, e, f, and g showed similar morphology as BEA zeolite. This observation indicated that the surface structure and amorphous identity of embryonic zeolite was unaltered after the deposition of Titania photocatalyst and only additional roughness on the surface was observed. Saadati et al. and Kanakaraju et al. attributed this roughness to the deposition of the TiO_2 particles as multi-sized clusters [23,26,43]. Fig. 3, h, shows the EDX elemental composition of the 60FeTZ photocatalyst and Fig. 3, i, j, k, l, n, and

Table 1
BET surface area (m^2/g), pore volume (cm^3/g), and crystallite size (nm) of BEA zeolite, TiO_2, and TiO_2/BEA ion-exchanged photocatalysts.

Catalyst	BET surface area (m^2/g)	External surface area (m^2/g)	Micro-pore volume (cm^3/g)	Meso-pore volume (cm^3/g)	Total Volume (cm^3/g)
TiO_2	32.94	30.62	0	0.089	0.098
BEA	389.78	326.15	0.028	0.917	0.945
60TZ	226.63	214.29	0.015	0.509	0.524
20FeTZ	278.38	227.1	0.013	0.595	0.608
40FeTZ	246.34	207.89	0.01	0.401	0.511
60FeTZ	214.36	189.40	0.008	0.419	0.427
100FeTZ	176.25	161.77	0.005	0.368	0.373

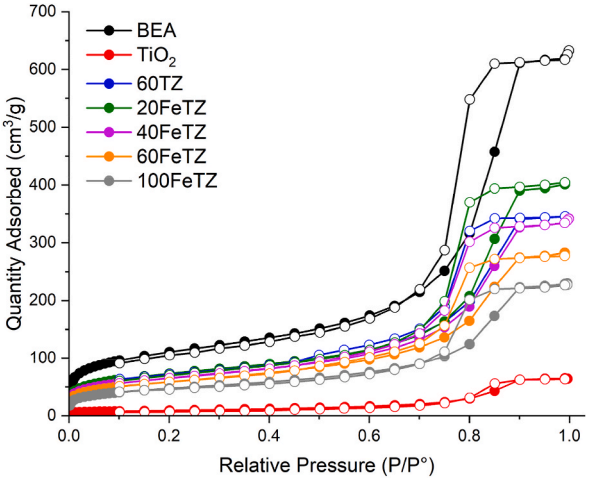

Fig. 2. N_2 Adsorption-Desorption Isotherm of BEA zeolite, TiO_2, TiO_2/BEA photocatalysts.

n exhibits the surface distribution of O, Al, Si, Ti, Na, and Fe atoms for this photocatalyst. The presence of all those elements on the surface of the final photocatalyst proved the immobilization of Titania over the BEA zeolite, and the presence of the iron after ion exchange.

3.1.2. Doping method

3.1.2.1. XRD analysis and TGA. The XRD patterns of the Fe doped-TiO_2/BEA photocatalysts showed very low crystallinity as compared to TiO_2 (Fig. 4). All TiO_2/BEA samples showed characteristic diffraction peak for the zeolite at $2\theta = 7.6°$ and for anatase TiO_2 at $2\theta = 25°$, 36.98°, 48.4°, 54.9°, 62.7° in a similar pattern as the ion-exchanged photocatalysts. This was also a clear proof that both zeolite and TiO_2 were present in the final photocatalysts, and that the framework structure of the zeolite was not altered. For the doped samples, most of the doped Titania was deposited on the surface of the zeolite as anatase polymorphs [15,16,24].

Fig. S3 shows the TGA thermograms of the doped Titania photocatalysts. As compared to 60TZ, the further addition of Fe dopant into the supported Titania caused a slight weight loss of less than 5 %. This still indicated that all the doped Titania photocatalysts were thermally stable between 35 °C and 1000 °C just like the ion-exchanged samples.

3.1.2. 1. Specific surface area (BET) and N_2 adsorption–desorption characterization. Table 2 summarized the BET results of the Fe-doped Titania photocatalysts. The final doped immobilized titania samples showed significant increase in the surface area and pore volume as compared to pure TiO_2 although part of the titania was deposited in the zeolite's pores [14,35]. The 3 % Fe doping showed a surface area of 241.4 m^2/g and a pore volume of 0.509 cm^3/g less than that of the 7FeTZ catalyst. This increase in the surface area and pore volume is due to the presence of Fe dopant ions which results in larger particle sizes of the doped titania, minimizing the probability of their deposition in the meso-pores of zeolite [44]. However, for the highest Fe content (10 %), the BET surface area decreased to 229.38 m^2/g while the pore volume increased to 0.571 cm^3/g indicating a lesser pore clogging. Based on Table 2, some of the doped photocatalysts possessed a larger surface area as compared to photocatalysts with the same zeolite content found in Table 1. As shown in (Fig. 5), the isotherms of all the Fe-doped TiO_2/BEA samples were type IV isothermals with hysteresis loops in accordance with the IUPAC isotherm classifications [36]. However, a conversion from H2 hysteresis to H1 hysteresis can be observed upon the deposition of doped Titania over the zeolite. This was a result of a minor change of the pore structure due to Fe doping [45].

3.1.2. 2. FTIR. The FTIR spectrum of the doped immobilized Titania photocatalysts was similar to that of the zeolite maintaining the same peaks but with lower intensities, Fig. S4. The modified catalysts also showed new close peaks around 2500 cm^{-1} that corresponded to TiO_2. From Fig. S4, a change in the shape of the FTIR of the doped catalysts between 500 cm^{-1} and 900 cm^{-1} with a very low intensity of the peak associated to the zeolite around 790 cm^{-1} can also be observed. This indicates strong interaction between the Titania particles and the external pores of the zeolite, similar to observations of other ion-exchanged photocatalysts [17,42]. As shown in the FTIR spectrum of the 3FeTZ sample between 940 and 980 cm^{-1}, we can observe a peak at 965 cm^{-1} with a very low intensity indicating a presence of Ti–O–Si bond. Therefore, it can be concluded that the solgel Titania photocatalyst was successfully immobilized over the amorphous BEA zeolite through chemical bonding while preserving the structure of zeolite.

3.1.2. 3. SEM surface morphology characterization and EDX mapping. The SEM images of the doped Titania photocatalysts possessed a similar morphology as BEA zeolite as shown in Fig. 6, a, b, and c. This indicated that the structure and morphology of the zeolite was conserved upon the deposition of the doped Titania that also formed clusters on the zeolite's surface similar to the ion-exchanged photocatalysts [23]. Fig. 6, d, shows the elemental composition of the 3FeTZ photocatalyst obtained from EDX while Fig. 6, e, f, g,

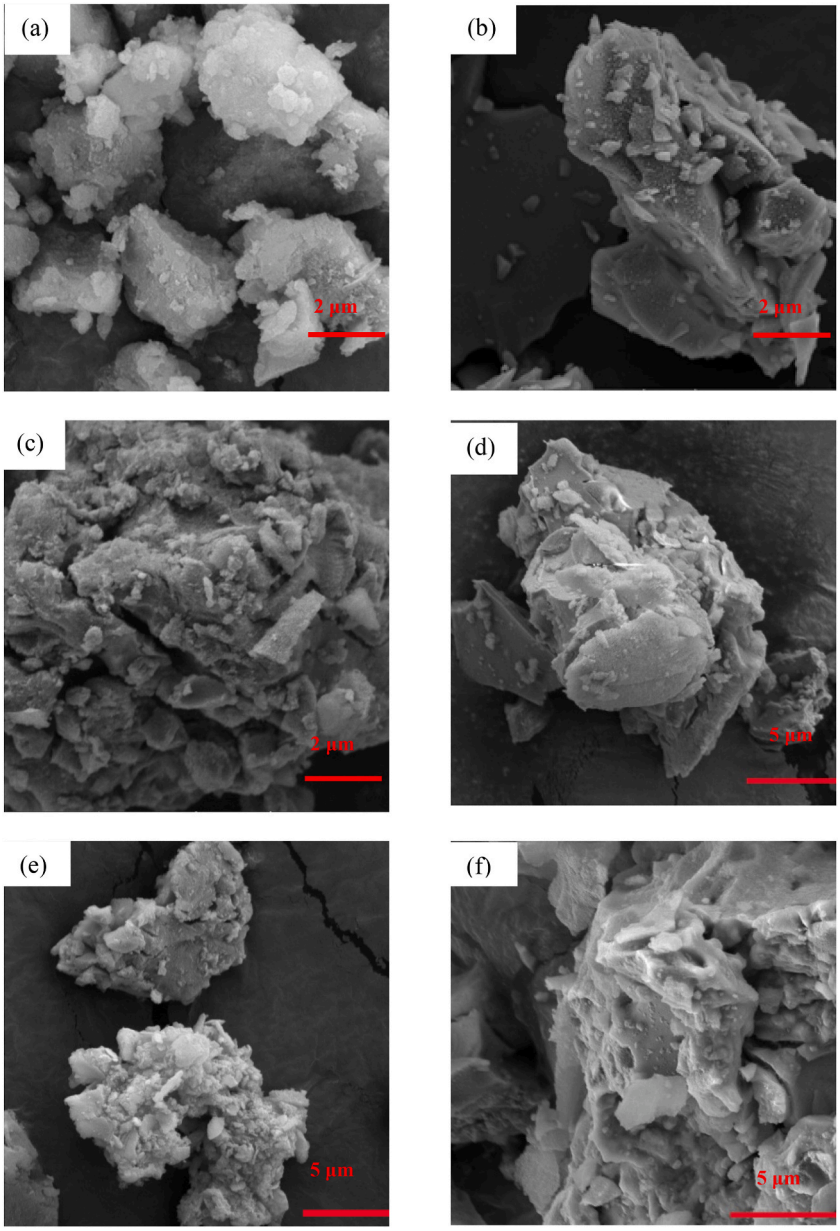

Fig. 3. SEM picture of (a) BEA, (b) TiO_2, (c) 60TZ, (d) 20FeTZ, (e) 40FETZ, (f) 60FETZ, (g) 100FETZ catalysts, (h) elemental analysis, (i) O, (j) Al, (k) Si, (l) Ti, (m) Na, and (n) Fe EDX mapping of 60FeTZ elements.

h, i, and j illustrate the distribution of Si, Al, Na, Ti, and Fe atoms on the surface of this photocatalyst. This was further evidence that doped Titania was successfully immobilized on the surface of the zeolite.

3.2. Experimental results

3.2.1. Ion exchange

3.2.1.1. Adsorption of tetracycline of tetracycline. Fig. 7 shows the adsorption percentages of tetracycline (TC) antibiotic into BEA zeolite, TiO_2, and Titania photocatalysts.

All the obtained adsorption plots followed type I adsorption isotherm characterized by a rapid rate at the beginning of the adsorption that slowed down to reach a plateau after a certain duration. Similar adsorption patterns were reported by Lui et al. [29]

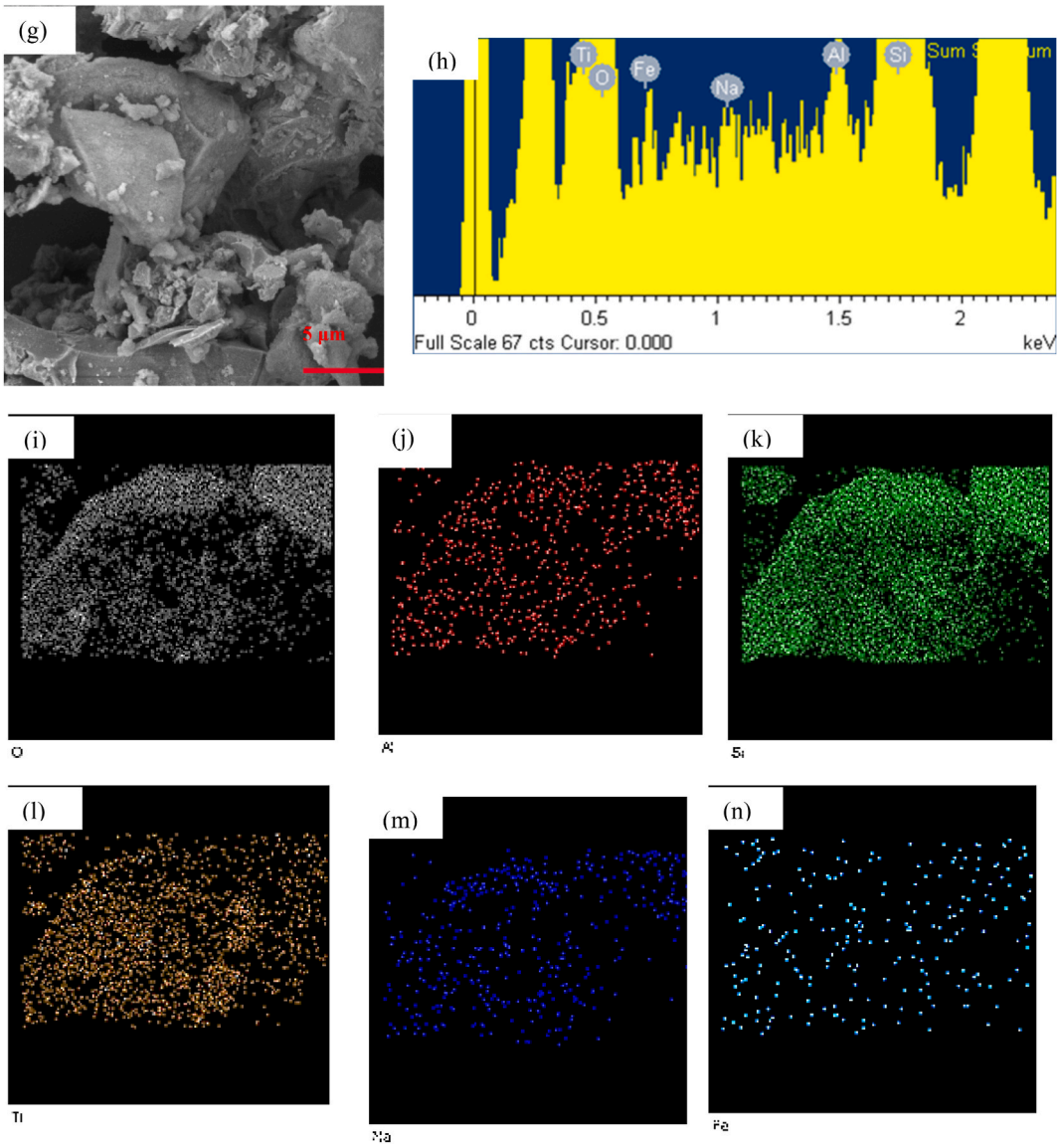

Fig. 3. (*continued*).

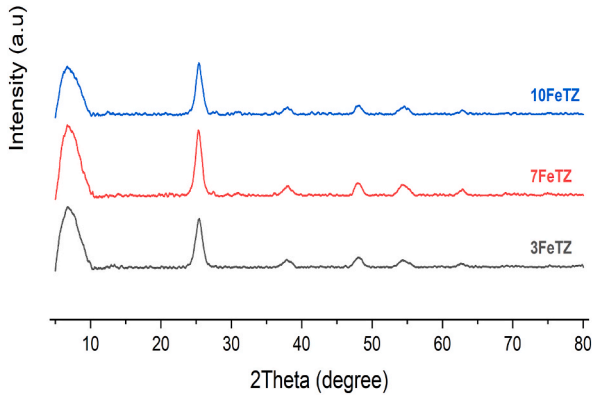

Fig. 4. XRD pattern of BEA, TiO_2, and Fe-doped TiO_2/BEA photocatalysts.

Table 2
BET surface area (m^2/g), pore volume (cm^3/g), and crystallite size (nm) of BEA, TiO_2, and Fe-doped TiO_2/BEA photocatalysts.

Catalyst	BET surface area (m^2/g)	External surface area (m^2/g)	Micro-pore volume (cm^3/g)	Meso-pore volume (cm^3/g)	Total Volume in Pores (cm^3/g)
3FeTZ	241.47	214.90	0.005	0.509	0.509
7FeTZ	260.88	192.88	0.002	0.466	0.468
10FeTZ	229.38	186.98	0.014	0.557	0.571

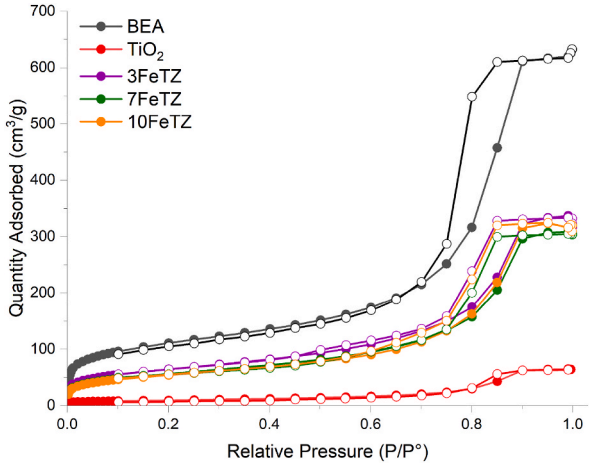

Fig. 5. N_2 Adsorption-Desorption Isotherm of BEA zeolite, TiO_2, and Fe-doped TiO_2/BEA photocatalysts.

who prepared TiO_2/BEA catalysts to degrade sulfadiazine antibiotic. After 5 h, TiO_2 was only able to degrade 8.22 % of the initial TC while BEA zeolite adsorbed 10.5 %. After the immobilization of TiO_2 over the BEA zeolite, its adsorption efficiency increased in the order 40FeTZ~60FeTZ~60TZ > 20FeTZ>100FeTZ > BEA > TiO_2. This resultant enhancement in the adsorption of TC was mainly attributed to the higher surface area and pore volume of the Titania photocatalysts as previously discussed in the BET section. For example, the 100FeTZ sample exhibited a lower surface area and accordingly resulted in a lower adsorption efficiency. The adsorption percentages of the remaining catalysts were around 17 %. This improved adsorption efficiency of the Titania photocatalysts was reported by other studies employing TiO_2 immobilized over porous zeolite [16,26]. The mechanism of TC adsorption by TiO_2 is highly controlled by the diffusion step and the presence of zeolite with the large surface area and porous structures facilitated this step. On the other hand, the adsorption of TC is linked to electrostatic interactions and bond formation between the functional groups in TiO_2 and the amide, carbonyl, and phenol groups found in TC [46]. Therefore, higher adsorption efficiency is a result of a better diffusion, guaranteed by higher surface area and pore volume in addition to better electrostatic interactions with TiO_2 imposed by higher concentrations of this photocatalyst. Accordingly, an optimal combination between the amount of TiO_2 and the amount of the zeolite will lead to the highest adsorption efficiency as obtained by the 40FeTZ photocatalyst.

3.2.1.2. Photocatalytic degradation of tetracycline under blue light. Under blue light that symbolizes the near visible region in the light spectrum, TiO_2 is very active as reported in literature because it exhibits a high band gap energy [47]. Therefore, many studies applied a variety of modification methods to improve the performance of TiO_2 under visible light by enhancing its visible light absorption [2,5,48]. As shown in Fig. 8, the degradation efficiency of TiO_2 under blue light was the highest as compared to the ion exchanged TiO_2/BEA photocatalysts. Since TiO_2 is highly active under blue light, its active sites were responsible for the degradation of TC through a high rate of electron excitation. The presence of zeolite in the photocatalyst led to a reduction in the number of active sites, however it improved the interaction between TC molecules and the active sites of Titania due to enhanced adsorption. Specifically, for an equivalent catalyst weight, the presence of zeolite resulted in a lower quantity of TiO_2 within the reaction medium, as indicated by the weight percentage of TiO_2 in the samples when compared to pure TiO_2. This decrease in TiO_2 content led to a reduced generation of excited electrons and consequently lesser degradation rate of tetracycline as per the proposed mechanism in Fig. 10.

3.2.1.3. Photocatalytic degradation of tetracycline under white light. White light indicates the solar spectrum and includes UV and visible light. Under white irradiations, TiO_2 exhibited lower activity as compared to the blue light due to its wide band gap and low visible light absorption according to Fig. 9. This meant that under white light, TiO_2 can only be activated by the UV part of the spectrum and degrade TC by radical formation due to electron excitation [49]. However, the iron ion exchanged was proven to be feasible to lower the band gap energy of the immobilized Titania photocatalyst and therefore enhance its visible light absorption [10]. Accordingly, the Fe ions can absorb the visible light and an excited electron can move from the Fe^{3+} ions into the conduction band of TiO_2 allowing the formation of the hydroxide radicals that can mineralize the TC molecules based on the localized surface plasmon resonance mechanism

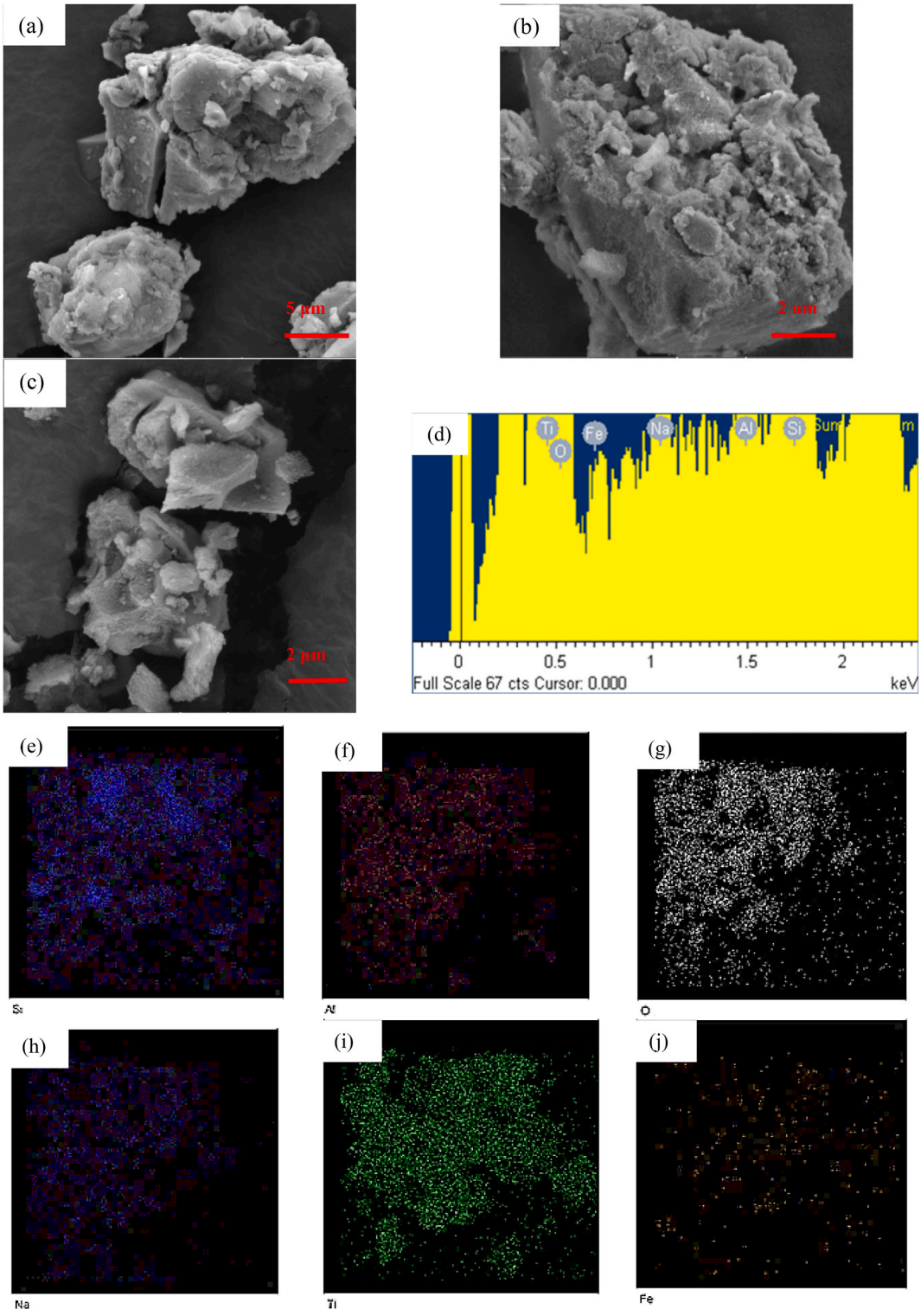

Fig. 6. SEM picture of (a) 3FeTZ, (d) 7FeTZ, (e) 10FeTZ doped photocatalysts, (f) elemental analysis, (g) Si, (h) Al, (i) O, (g) Na, (k)Ti, and (l) Fe EDX mapping of 3FeTZ elements.

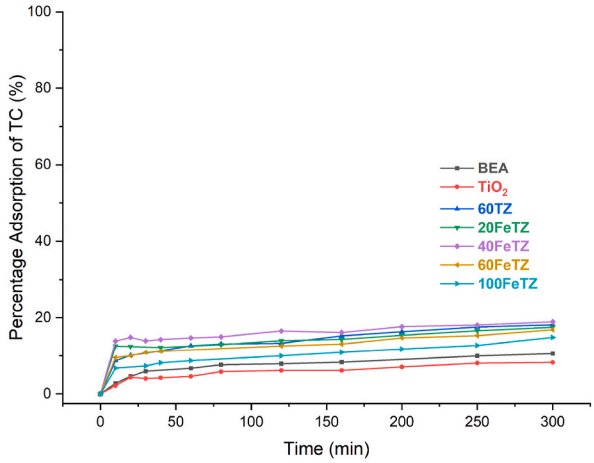

Fig. 7. Adsorption efficiency of BEA, TiO_2, and ion-exchanged TiO_2/BEA photocatalysts 100 mg/L dose and 20 ppm TC concentration.

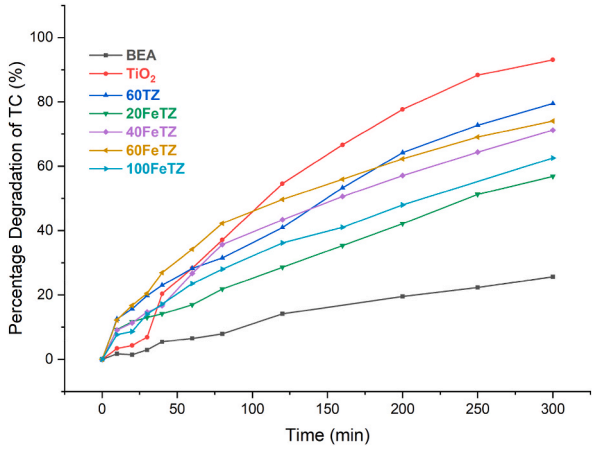

Fig. 8. Photocatalytic degradation efficiencies under blue LED light for BEA, TiO_2, and ion-exchanged TiO_2/BEA photocatalysts with 100 mg/L dose and 20 ppm TC concentration.

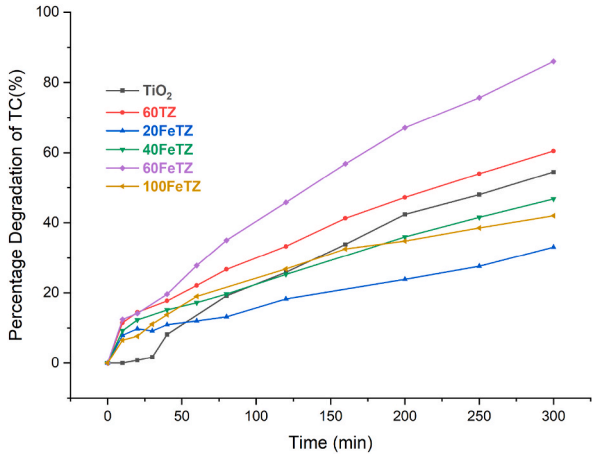

Fig. 9. Photocatalytic degradation efficiencies BEA, TiO_2, and ion-exchanged TiO_2/BEA photocatalysts under white LED light and 20 ppm TC concentration and 100 mg/L photocatalyst dose.

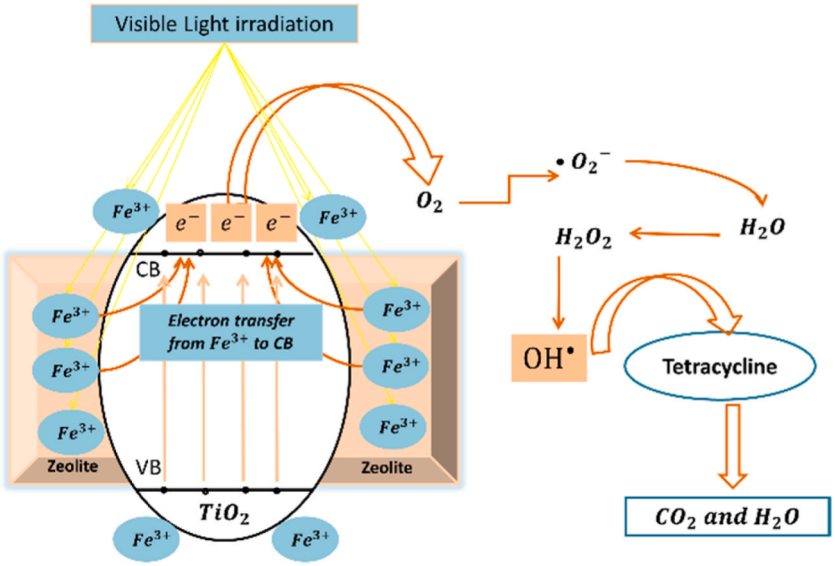

Fig. 10. The proposed mechanism of TC degradation by TiO_2/BEA ion-exchanged photocatalysts under visible light.

as mentioned by Maksod et al. [31] and as presented in Fig. 10. Based on Fig. 9, the highest degradation efficiency was obtained by the 60FeTZ sample with around 85 % degradation after 300 min compared to only 54 % by TiO_2. The higher degradation efficiency of 60FeTZ as compared to 60TZ was due to the presence of the Fe ions in the photocatalyst that had enhanced its visible light absorption. Previous studies using immobilized TiO_2 showed an improved degradation activity of Titania photocatalysts as compared to Titania due to the suppression in the recombination of the charge carriers [17]. Where, this was the reason for the slight enhanced degradation efficiency of 60TZ as compared to TiO_2. Particularly, the surface of the zeolite can be saturated with excited electron that are capable of entrapping the positive holes and minimize the charge carrier recombination rate [17]. Additionally, zeolite immobilization may minimize the adverse effect of Titania aggregation in solution due to uniform distribution on its surface [10]. Accordingly, the excellent performance of 60FeTZ as compared to TiO_2 was a result of zeolite acting as electron trapper and improving adsorption as well as ion exchange with ferric ions that decreased the band gap energy of Titania and enhanced its visible light absorption. For the other Titania photocatalysts, they all resulted in degradation efficiencies less than that of TiO_2. Under white light, both TiO_2 and the Fe content play important role in the degradation mechanism as illustrated in Fig. 10. Higher Fe content could lead to higher visible light absorption and this happened when the weight percentage of TiO_2 was low and zeolite content was high in 20FeTZ [6]. However, this photocatalyst degraded the least amount of TC and this could be a result of not enough active sites in TiO_2. The opposite was encountered in the 100FeTZ sample. Where, the Fe content was lower and the active sites of TiO_2 were greater for a higher weight percentage. Based on our results, the efficiency of this photocatalyst was also low and this could be due to minimal visible light absorption due to low Fe content and therefore lesser number of excited electrons [5]. Accordingly, there should be an optimal weight percentage of TiO_2 that allows enough Na^+ ions in zeolite to be exchanged with Fe sensitizing metal ions to improve its visible light absorption. Rahman et al. [17] prepared TiO_2/natural zeolite photocatalyst for the degradation of methyl orange dye under solar light. In this study, when the weight percentage of TiO_2 was 2.5 % and 5 %, the performance of the immobilized Titania was less than that of TiO_2 and showed an unstable trend. However, when the weight percentage of TiO_2 was 10 %, the efficiency of the photocatalyst was much higher than TiO_2.

3.2.2. *Doping*

3.2.2.1. Adsorption of tetracycline of tetracycline. Fig. 11 shows the adsorption of tetracycline antibiotic by Fe doped-TiO_2/BEA photocatalysts. The adsorption efficiency of Titania was nearly doubled for the doped TiO_2/BEA photocatalysts. This enhanced adsorption efficiency was mainly due to the increase in the surface area and pore volume of the photocatalysts as previously indicated by the BET analysis. The 7FeTZ exhibited the highest surface area (260.88 m^2/g) and the highest final adsorption percentage (24 %). Similarly, the 10FeTZ resulted in the same adsorption percentage while having the highest pore volume. The adsorption efficiencies of the doped catalysts were higher than the efficiencies of the ion-exchanged photocatalysts as a result of higher surface area or higher pore volume for the same weight percentage of TiO_2.

3.2.2.2. Photocatalytic degradation of tetracycline under blue light. As presented in Fig. 12, we observed that among the Fe-doped photocatalysts, only 3FeTZ resulted in a final efficiency higher than that of TiO_2 (97 %) and only 17 % of TC were degraded in the absence of any catalyst. This slight enhancement in the TiO_2 performance under blue light was mainly due to the fact that blue light represents near visible region and not a totally visible light where TiO_2 is known to have a very low activity [47].

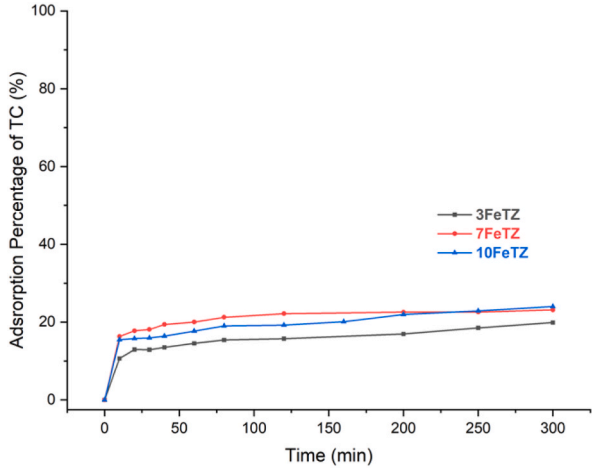

Fig. 11. Adsorption efficiency of BEA, TiO_2, and Fe-doped TiO_2/BEA photocatalysts with 100 mg/L dose and 20 ppm TC concentration.

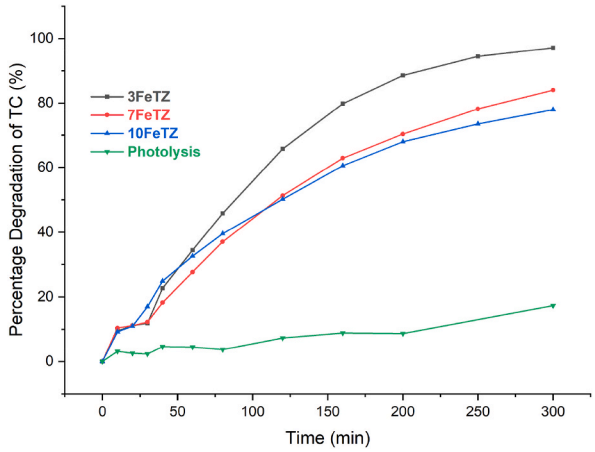

Fig. 12. Photocatalytic degradation efficiencies under blue LED light for BEA, TiO_2, and Fe-doped TiO_2/BEA photocatalysts with 100 mg/L dose and 20 ppm TC concentration.

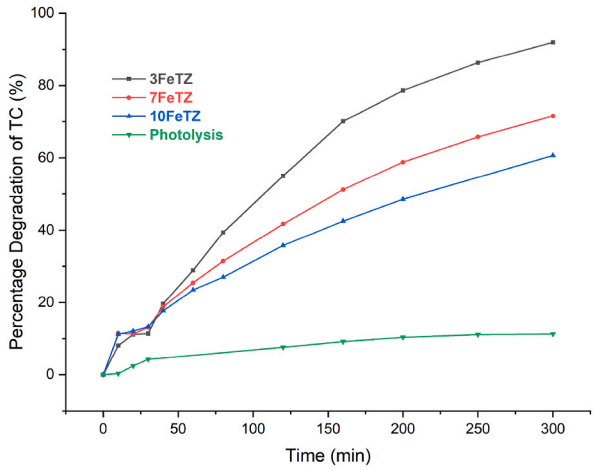

Fig. 13. Photocatalytic degradation efficiencies under white LED light for BEA, TiO_2, and Fe-doped TiO_2/BEA photocatalysts with 100 mg/L dose and 20 ppm TC concentration.

3.2.2.3. Photocatalytic degradation of tetracycline under white light. As shown in Fig. 13, under white light, considered a simulator of solar spectrum, all the Titania photocatalysts showed better degradation efficiencies as compared to the unmodified TiO_2. After 300 min, TiO_2 only degraded 50 % of the initial TC in solution compared to 92 % by 3FeTZ, 71 % by 7FeTZ, and 61 % by 10FeTZ compared to only 11 % in the absence of any catalyst. Foura et al. and Ali et al. [5,7] reported a decrease in the band gap energy of TiO_2 when increasing the iron doping concentration and Foura et al. observed an enhanced photocatalytic performance upon increasing the Fe weight percent up to an optimal value beyond which the performance deteriorates. In our study, the presence of higher Fe content (7 % and 10 %) led to lower efficiencies than 3FeTZ due to the presence of excess trapping species in the transfer route of charger carriers that caused a slower movement of electrons [7]. Accordingly, for our application, the 3 % by mole TiO_2/BEA was the optimal doping concentration. In comparison to the ion-exchanged photocatalysts, the doped photocatalysts exhibited superior performance when exposed to white light. This observation suggests that doping serves as a more effective sensitization method for augmenting the visible light activity of immobilized Titania.

Iron doping had been widely applied for Titania to enhance its visible light absorption and photocatalytic degradation performance [5,7]. The Fe doping was proven not only to lower the band gap energy of TiO_2 and consequently enhance its visible light absorption, but to also suppress the recombination effect of charge carrier (e^-/h^+) pairs when used in an optimal concentration [5–7]. We herein describe the role of Fe ions on the photocatalytic degradation of TC. In the Fe-doped TiO_2, two kinds of energy levels were created. A reduction level characterized by Fe^{3+}/Fe^{2+} located above the valence band of TiO_2, and an oxidation level characterized by $\mathbf{Fe^{4+}/Fe^{3+}}$ located below the conduction band of TiO_2 [5]. During the photocatalytic reaction, unstable $\mathbf{Fe^{2+}}$ ions were created due to the migration of electrons from the conduction band of TiO_2. Fe^{2+} would be transformed back to Fe^{3+} as a result of oxidation reaction with oxygen molecules that also created highly reactive superoxide ions $\mathbf{O_2^-}$. The presence of Fe^{3+} dopant ion helped minimize the recombination effect of charge carriers by entrapping the positive holes $\mathbf{h}^+$ and creating Fe^{4+}. The created Fe^{4+} would then convert OH^- ions into hydroxide radicals ·OH and $\mathbf{Fe^{3+}}$. The hydroxide and super oxide reactive species were responsible for tetracycline degradation [2] as shown in Fig. 14.

3.2.3. Photocatalytic degradation of tetracycline under real solar irradiations

Fig. 15 shows the photocatalytic degradation of TC under real solar irradiations by TiO_2, 60FeTZ, and 3FeTZ. When testing the most efficient catalysts 60FeTZ and 3FeTZ under real solar irradiations, TC complete degradation occurred after only 150 min by 3FeTZ compared to 200 min by 60FeTZ and while approximately 97 % degradation was achieved by the unmodified TiO_2 after 300 min. This indicated that 3FeTZ was the optimal photocatalyst among all doped and ion exchanged photocatalysts. As compared to white LED light, the efficiencies of both TiO_2 and modified TiO_2 were higher. This was due to higher energy and intensity of the solar light as compared to the low power of LED light used (50W). Similar finding was also reported by Chen et al. [50] who reported improved photocatalytic degradation of trichloroethylene as the power of the LED light increased. In this study by Chen et al., the improvement in the activity of the Titania was justified by the increase in the number of active hydroxide radicals as a result of stronger excitation energy provided by the light. For TC photocatalytic degradation, Das et al. [51] compared the efficiency of CdS nanorods under 50 and 200 (W/m^2) light intensities. The final removal efficiency after 60 min increased from 60.5 % to 80.1 %. Based on this information from similar studies and as illustrated in the proposed mechanisms in Figs. 10 and 14, more TC molecules will be degraded and higher activity of the photocatalyst will be obtained to increased number of excited electrons. The photocatalytic degradation results under solar irradiations are in consistence with those under white light. The best performing photocatalyst under white LED light was the 3FeTZ followed by 60FeTZ. The enhanced performance of the doped and ion exchanged samples were explained based on the mechanism of degradation in the previous sections.

4. Conclusion

In this study, we synthesized Fe-sensitized TiO_2 immobilized over embryonic BEA zeolite for the photocatalytic degradation of tetracycline antibiotic under visible light. The XRD, SEM, EDX, FTIR, and BET confirmed the deposition of the doped Titania mainly on

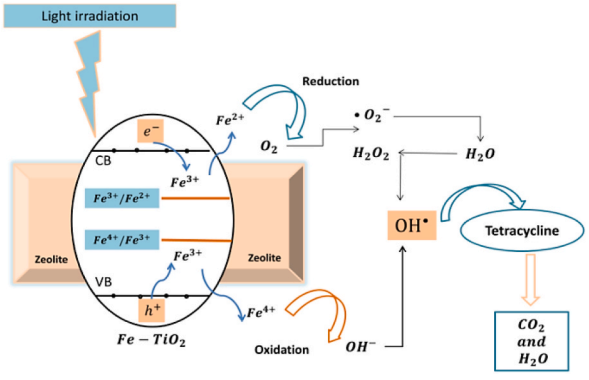

Fig. 14. The proposed mechanism of TC degradation by Fe-doped TiO_2/BEA photocatalyst under visible light.

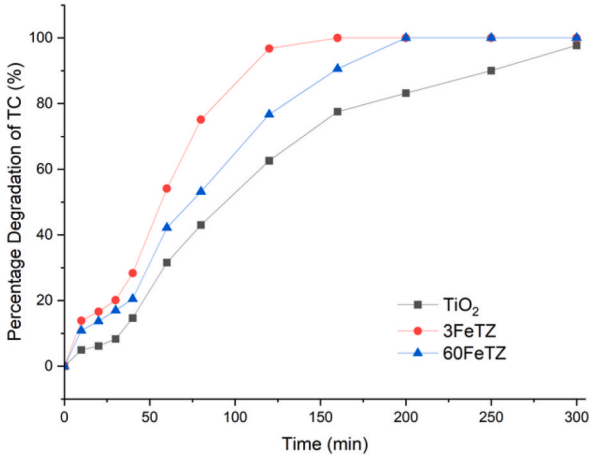

Fig. 15. Photocatalytic degradation efficiencies of TC by TiO_2, 60FETZ, and 3FeTZ photocatalysts under real solar radiation with 100 mg/L photocatalyst dose and 20 ppm TC concentration.

the surface of the amorphous zeolite. Under dark conditions, the adsorption tests indicated that using zeolite as a support for Titania enhanced its adsorption efficiency towards pollutants and this was a result of the increase in the surface area of the Titania photocatalysts. Under white light, all doped TiO_2/BEA samples possessed better efficiencies as compared to ion exchanged samples and TiO_2 with 3FeTZ being the optimal photocatalyst. 3FeTZ was also observed as the best performing photocatalyst when tested under real solar irradiations. This improvement in the performance of Titania was a result of both enhanced adsorption due to zeolite and increased visible light harvesting due to Fe metal doping that was known to minimize the band gap energy, entrap the excited charge carriers (e^-/h^+ pairs), and suppress the recombination effect. We also conclude that using an amorphous large surface area zeolite, prepared easier and quicker than the crystalline, as a support for Titania was successful. Metal doped TiO_2 immobilized over amorphous zeolite with high surface area and high pore volume can be a promising method to develop a visible light active photocatalyst for degrading organic and pharmaceutical pollutants.

Data availability statement

We hereby declare that the data associated with this study has not been deposited into a publicly available repository. We have also included the remaining information in a supplementary document. Data are available by the corresponding author upon reasonable request.

CRediT authorship contribution statement

Ghadeer Jalloul: Writing – original draft, Methodology, Data curation, Conceptualization. **Nour Hijazi:** Resources, Methodology. **Cassia Boyadjian:** Writing – review & editing, Supervision, Conceptualization. **Hussein Awala:** Supervision, Methodology, Conceptualization. **Ahmad Albadarin:** Writing – review & editing, Supervision, Project administration, Data curation. **Mohammad N. Ahmad:** Writing – review & editing, Supervision, Project administration, Funding acquisition.

Declaration of competing interest

The authors declare that they have no known competing financial interests or personal relationships that could have appeared to influence the work reported in this paper.

Appendix A. Supplementary data

Supplementary data to this article can be found online at https://doi.org/10.1016/j.heliyon.2024.e31854.

References

[1] D.G.J. Larsson, C.-F. Flach, Antibiotic resistance in the environment, Nat. Rev. Microbiol. 20 (5) (2022) 257–269.
[2] G. Jalloul, et al., Antibiotics contaminated irrigation water: an overview on its impact on edible crops and visible light active titania as potential photocatalysts for irrigation water treatment, Front. Environ. Sci. 9 (642) (2021).
[3] I. Sutradhar, et al., Effects of antibiotic interaction on antimicrobial resistance development in wastewater, Sci. Rep. 13 (1) (2023) 7801.

[4] L. Xu, et al., Occurrence, fate, and risk assessment of typical tetracycline antibiotics in the aquatic environment: a review, Sci. Total Environ. 753 (2021) 141975.
[5] T. Ali, et al., Photocatalytic performance of Fe-doped TiO2nanoparticles under visible-light irradiation, Mater. Res. Express 4 (1) (2017) 015022.
[6] A. Tsiampalis, et al., Degradation of sulfamethoxazole using iron-doped titania and simulated solar radiation, Catalysts 9 (7) (2019) 612.
[7] G. Foura, et al., Fe-doped TiO2 supported on HY zeolite for solar photocatalytic treatment of dye pollutants, Catalysts 7 (11) (2017) 344.
[8] P. Wang, P.-S. Yap, T.-T. Lim, C–N–S tridoped TiO2 for photocatalytic degradation of tetracycline under visible-light irradiation, Appl. Catal. Gen. 399 (1) (2011) 252–261.
[9] S.M. Ghoreishian, et al., Tuning the phase composition of 1D TiO2 by Fe/Sn co-doping strategy for enhanced visible-light-driven photocatalytic and photoelectrochemical performances, J. Alloys Compd. 851 (2021) 156826.
[10] G. Jalloul, et al., Fe-sensitized zeolite supported TiO2 for the degradation of tetracycline using blue LED irradiation, Front. Environ. Sci. 10 (2022).
[11] S.N.H. Arifin, et al., Modified TiO_2 nanotubes-zeolite composite photocatalyst: characteristics, microstructure and applicability for degrading triclocarban, Chemosphere 287 (Pt 3) (2022) 132278.
[12] T. Kurniawan, et al., BaTiO 3/TiO 2 composite-assisted photocatalytic degradation for removal of acetaminophen from synthetic wastewater under UV–vis irradiation, Mater. Sci. Semicond. Process. 73 (2017).
[13] L. Yanyan, et al., Enhanced photocatalytic degradation of acetaminophen from wastewater using WO 3/TiO 2/SiO 2 composite under UV–VIS irradiation, J. Mol. Liq. (2017) 243.
[14] S. Behravesh, et al., Photocatalytic degradation of acetaminophen and codeine medicines using a novel zeolite-supported TiO2 and ZnO under UV and sunlight irradiation, Environ. Sci. Pollut. Control Ser. 27 (21) (2020) 26929–26942.
[15] R.J. Tayade, R.G. Kulkarni, R.V. Jasra, Enhanced photocatalytic activity of TiO2-coated NaY and HY zeolites for the degradation of methylene blue in water, Ind. Eng. Chem. Res. 46 (2) (2007) 369–376.
[16] N. Saqib, R. Adnan, I. Shah, Zeolite supported TiO2 with enhanced degradation efficiency for organic dye under household compact fluorescent light, Mater. Res. Express 6 (2019).
[17] A. Rahman, et al., Enhanced activity of TiO2/natural zeolite composite for degradation of methyl orange under visible light irradiation, International Journal of Technology 9 (2018) 1159.
[18] A. Palčić, et al., Embryonic zeolites for highly efficient synthesis of dimethyl ether from syngas, Microporous Mesoporous Mater. 322 (2021) 111138.
[19] K.-G. Haw, et al., Embryonic ZSM-5 zeolites: zeolitic materials with superior catalytic activity in 1,3,5-triisopropylbenzene dealkylation, New J. Chem. 40 (5) (2016) 4307–4313.
[20] M. Akouche, et al., Synthesis of embryonic zeolites with controlled physicochemical properties, Chem. Mater. 32 (5) (2020) 2123–2132.
[21] L. Wang, et al., Embryonic zeolite-assisted synthesis of SSZ-13 with superior efficiency and their excellent catalytic performance, J. Mater. Chem. A 9 (27) (2021) 15238–15245.
[22] F. Saadati, N. Keramati, M.M. Ghazi, Influence of parameters on the photocatalytic degradation of tetracycline in wastewater: a review, Crit. Rev. Environ. Sci. Technol. 46 (8) (2016) 757–782.
[23] D. Kanakaraju, et al., Titanium dioxide/zeolite integrated photocatalytic adsorbents for the degradation of amoxicillin, Appl. Catal. B Environ. (2014) 166–167.
[24] M. Liu, et al., Degradation of ciprofloxacin by TiO2/Fe2O3/zeolite catalyst-activated persulfate under visible LED light irradiation, RSC Adv. 7 (81) (2017) 51512–51520.
[25] K. Wang, et al., Crystalline phase regulation of anatase–rutile TiO2 for the enhancement of photocatalytic activity, RSC Adv. 10 (71) (2020) 43592–43598.
[26] F. Saadati, N. Keramati, M. Mehdipour ghazi, Synthesis of nanocomposite based on Semnan natural zeolite for photocatalytic degradation of tetracycline under visible light, Advances in Environmental Technology 2 (2) (2016) 63–70.
[27] J.G. Piedra López, et al., Photocatalytic degradation of metoprolol in aqueous medium using a TiO2/natural zeolite composite, Fuel 284 (2021) 119030.
[28] A. Ebrahimi, et al., The performance of TiO2/NaY-zeolite nanocomposite in photocatalytic degradation of Microcystin-LR from aqueous solutions: optimization by response surface methodology (RSM), Environmental Health Engineering and Management Journal 7 (4) (2020) 245–256.
[29] X. Liu, et al., Performance and mechanism into TiO2/Zeolite composites for sulfadiazine adsorption and photodegradation, Chem. Eng. J. 350 (2018) 131–147.
[30] S. Shokrolahi, M. Farhadian, N. Davari, Degradation of Enrofloxacin antibiotic in contaminated water by ZnO/Fe2O3/Zeolite nanophotocatalyst, Journal of Applied Research in Water and Wastewater 6 (2) (2019) 150–155.
[31] I.H.A.E. Maksod, et al., Structural and photocatalytic properties of precious metals modified TiO2-BEA zeolite composites, Mol. Catal. 441 (2017) 140–149.
[32] M. Liu, et al., Removal of oxytetracycline by Fe2O3–TiO2/modified zeolite composites under visible light irradiation, J. Mater. Sci. Mater. Electron. (2019) 30.
[33] L. Price, K.M. Leung, A. Sartbaeva, Local and average structural changes in zeolite A upon ion exchange, Magnetochemistry 3 (4) (2017) 42.
[34] A. Gęsikiewicz-Puchalska, et al., Changes in porous parameters of the ion exchanged X zeolite and their effect on CO2 adsorption, Molecules 26 (24) (2021) 7520.
[35] C. Sun, et al., Study on preparation and visible-light activity of Ag–TiO2 supported by artificial zeolite, Res. Chem. Intermed. 44 (4) (2018) 2607–2620.
[36] K.S.W. Sing, Reporting physisorption data for gas/solid systems with special reference to the determination of surface area and porosity (Recommendations 1984), Pure Appl. Chem. 57 (4) (1985) 603–619.
[37] N. Taufiqurrahmi, A.R. Mohamed, S. Bhatia, Nanocrystalline zeolite beta and zeolite Y as catalysts in used palm oil cracking for the production of biofuel, J. Nanoparticle Res. 13 (8) (2011) 3177–3189.
[38] M. Boroglu, M. Gürkaynak, Fabrication and characterization of silica modified polyimide–zeolite mixed matrix membranes for gas separation properties, Polym. Bull. 66 (2011) 463–478.
[39] M.N. Chong, et al., Synthesis, characterisation and application of TiO2–zeolite nanocomposites for the advanced treatment of industrial dye wastewater, J. Taiwan Inst. Chem. Eng. 50 (2015) 288–296.
[40] Y. Bouachiba, et al., TiO2 thin films studied by FTIR, AFM and spectroscopic ellipsometry, Int. J. Nanoparticles (IJNP) 6 (2013) 169–177.
[41] S. Bhat, R. Naikoo, N. Kumar, Synthesis of N-formylation of amines using various ion exchanged forms of zeolite-A as catalysts, Pharmacy & Pharmacology International Journal 5 (2017).
[42] F. Li, et al., Surface effect of natural zeolite (clinoptilolite) on the photocatalytic activity of TiO2, Appl. Surf. Sci. 252 (2005) 1410–1416.
[43] N. Aghajari, et al., Synthesis, characterization and photocatalytic application of Ag-doped Fe-ZSM-5@TiO2 nanocomposite for degradation of reactive red 195 (RR 195) in aqueous environment under sunlight irradiation, Journal of Environmental Health Science and Engineering 17 (1) (2019) 219–232.
[44] M.J. Valero-Romero, et al., Photocatalytic properties of TiO2 and Fe-doped TiO2 prepared by metal organic framework-mediated synthesis, Chem. Eng. J. 360 (2019) 75–88.
[45] Y. Yang, C. Tian, Synthesis and characterization of Fe-doped sulfated titania with high photocatalytic activity in visible light, Res. Chem. Intermed. 41 (8) (2015) 5271–5281.
[46] M. Brigante, P.C. Schulz, Remotion of the antibiotic tetracycline by titania and titania–silica composed materials, J. Hazard Mater. 192 (3) (2011) 1597–1608.
[47] T. Putta, M.-C. Lu, J. Anotai, Photocatalytic activity of tungsten-doped TiO2 with hydrothermal treatment under blue light irradiation, J. Environ. Manag. 92 (9) (2011) 2272–2276.
[48] I. Altin, M. Sökmen, Z. Bıyıklıoğlu, Sol gel synthesis of cobalt doped TiO2 and its dye sensitization for efficient pollutant removal, Mater. Sci. Semicond. Process. 45 (2016) 36–44.
[49] T. Suwannaruang, et al., Visible light-induced degradation of antibiotic ciprofloxacin over Fe–N–TiO2 mesoporous photocatalyst with anatase/rutile/brookite nanocrystal mixture, J. Photochem. Photobiol. Chem. 391 (2020) 112371.
[50] C.-J. Chen, et al., Treatment of trichloroethylene with photocatalyst-coated optical fiber, Water 11 (11) (2019) 2391.
[51] S. Das, Y.-H. Ahn, Synthesis and application of CdS nanorods for LED-based photocatalytic degradation of tetracycline antibiotic, Chemosphere (2021) 132870.